Measurement of Interpeptidic CuII Exchange Rate Constants of CuII -Amyloid-β Complexes to Small Peptide Motifs by Tryptophan Fluorescence Quenching

Cheryle N Beuning, Luca J Zocchi, Kyangwi P Malikidogo, Charlène Esmieu, Pierre Dorlet, Debbie C Crans, Christelle Hureau

Measurement of Interpeptidic Cu^{II} Exchange Rate Constants of Cu^{II}-Amyloid-beta Complexes to Small Peptide Motifs by Tryptophan Fluorescence Quenching

Cheryle N. Beuning [a], Luca J. Zocchi [a], Kyangwi P. Malikidogo[b], Charlène Esmieu[b], Pierre Dorlet[c], Debbie C. Crans *[a] and Christelle Hureau *[b]

[a] Department of Chemistry, Colorado State University, Fort Collins, CO 80525
[b] LCC-CNRS, Université de Toulouse, CNRS, Toulouse, France
[c] CNRS, Aix-Marseille Université, Laboratoire de Bioénergétique et Ingénierie des Protéines, IMM, Marseille, France.

Abstract: The interpeptidic Cu^{II} exchange rate constants were measured for two Cu amyloid-beta complexes, Cu($A\beta_{1-16}$) and Cu($A\beta_{1-28}$), to fluorescent peptides GHW and DAHW using a quantitative tryptophan fluorescence quenching methodology. The second-order rate constants were determined at three pH values (6.8, 7.4, and 8.7) important to the two Cu(Aβ) coordination complexes, components $Cu(A\beta)_I$ and $Cu(A\beta)_{II}$. The interpeptidic Cu^{II} exchange rate constants are approximately 10^4 $M^{-1}s^{-1}$ but vary in magnitudes depending on many variables. These include the pH, the length of the Aβ peptide, the location of the anchoring histidine ligand in the fluorescent peptide, the number of amide deprotonations required in the tryptophan peptide to coordinate the Cu^{II}, and the interconversion between $Cu(A\beta)_I$ and $Cu(A\beta)_{II}$. As the nonfluorescent GHK and DAHK peptides are important motifs found in the blood and serum, their ability to sequester Cu^{II} ions from Cu(Aβ) complexes may be relevant for the metal homeostasis and its implication in Alzheimer's disease. Thus, their kinetic Cu^{II} interpeptidic exchange rate constants are important chemical rate constants that can help elucidate the complex Cu^{II} trafficking puzzle in the synaptic cleft.

Alzheimer's disease (AD) pathology is extremely complex, and efforts to understand the many senile plaque formation mechanisms have been studied for decades. The beta-amyloid peptide, Aβ, was first sequenced in the 1980s and was the primary component of the senile plaques, leading to atrophy of neurons.[1-2] As the synaptic cleft space becomes riddled with precipitated Aβ protein, the neurons atrophy, which results in the hallmark AD symptoms such as dementia, memory loss, and ultimately death. The Aβ peptide can form innocuous soluble monomers from its cleavage from the amyloid precursor protein (APP), which does not seem to contribute to disease mechanisms. However, they can assemble into toxic oligomeric species, large unorganized aggregates, highly organized β-sheet fibrils, and bind metal ions with high affinity to form complexes, all of which can eventually amass into the senile plaques, which are a hallmark of AD.[3-12] Indeed, pathogenic Aβ is on a spectrum, where toxicity is often due to mechanisms that increase Aβ production and decrease Aβ clearance compared to normal healthy levels. Even though we all create the peptide, there is no guarantee it will develop into senile plaques.

One type of Aβ aggregation is metal-driven since Cu^{II}, Zn^{II}, and Fe^{II} ions are present within the synaptic cleft space. Concentrations of Cu^{II}, Zn^{II}, and Fe^{II} ions up to 400, 950, and 1100 μM[13], respectively, have been found in AD plaques.[3, 5, 7-10, 14] The coordination of these metals to the Aβ peptide has shown an altered propensity of it to aggregate and precipitate into senile plaques.[10, 15] Of particular interest is Cu^{II} which has a high affinity for the Aβ peptides, with association constants of 1×10^{10} M^{-1} at pH 7.4 for 1:1 Cu(Aβ) complexes.[3] Cu^{II} is a fascinating neurological metal as it is involved in a wide range of biologically essential processes.[16-19] Especially redox functions like mitochondrial oxidative phosphorylation within the brain.[17] We focused on Cu^{II} exchange in this work due to its high affinity for Aβ and its ability to quench tryptophan fluorescence.[20-25]

The Aβ peptide has many isoforms.[26] The lengths that are most associated with aggregation mechanisms are $A\beta_{1-40}$ (major form) and $A\beta_{1-42}$ (minor form).[4, 6, 27] The $A\beta_{1-42}$ isoform is more prone to aggregate than $A\beta_{1-40}$.[27] The cleavage of the APP is not highly specific. Small length isoforms like $A\beta_{1-16}$ and $A\beta_{1-28}$ are also observed (DAEFRHDSGYEVHHQK[16-

LVFFAEDVGSNK[28]). The Aβ peptide has a well-known metal-binding domain in the first 16 residues and is rich with nitrogen-donor ligands. The binding ligands include amide N^- (deprotonated amide NH to allow for coordination), imidazole histidine (His) N_{im}, and terminal NH_2, as well as oxygen-donor ligands like amide C=O and carboxylate groups (COO^-). The most accepted coordination position of the COO^- groups are in apical position, possibly via hydrogen bond to a water molecule.[28] For Cu(Aβ) complexes, at stoichiometric Cu^{II} to peptide ratio, monomeric species are largely predominant.[29] In addition, two major components are in equilibrium at physiological pH, which has pH-dependent coordination chemistry.[5, 7, 26, 30-33] $Cu(Aβ)_I$ is the predominant form at pH 6.8 where the Cu^{II} is bound to the NH_2, an amide C=O from Asp1, and two His N_{im}, **Figure 1**. Among the three possible His couples, the His6 and His13 or His14 are the most populated.[34] $Cu(Aβ)_{II}$ is predominant at pH 8.7 where the Cu^{II} coordinates to the NH_2 from Asp1, amide N^- and amide C=O from Ala2, and one His (His 6/13/14) N_{im} with no strong preference for any of the His residues, **Figure 1**. These binding sites correspond to the equatorial ligands, which are the most important for Cu^{II} coordination chemistry and will thus be those considered in the studies.

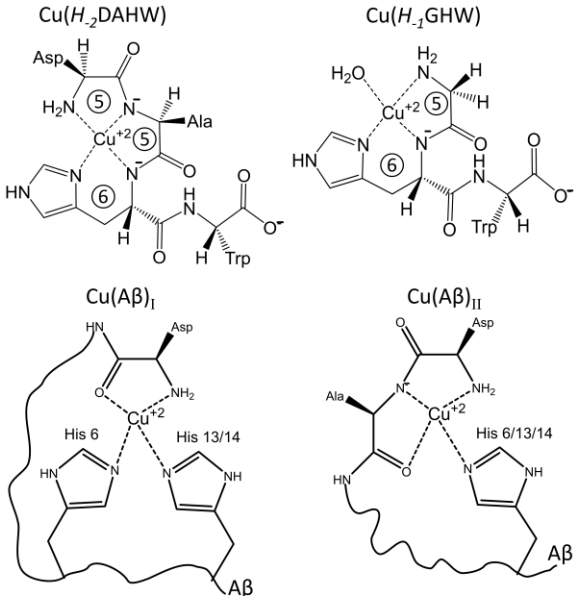

Figure 1: Solution structures of Cu(*H*-2DAHW), Cu(*H*-1GHW), $Cu(Aβ)_I$, and $Cu(Aβ)_{II}$ complexes. The Cu^{II} peptide binding sites form stable coordination complexes with adjacent 5 or 6 membered rings for the Trp-containing peptides.

The full-length Aβ peptides are significantly more challenging to work with due to their rapid aggregation mechanisms and their hydrophobic residues that predominate after Lys16. The $Aβ_{1-16}$ and $Aβ_{1-28}$ isoforms do not aggregate like the full-length $Aβ_{1-40/42,}$ but they both retain the metal-binding domain and are why they are used to study Cu^{II} binding in this work.

The DAHK peptide has biological relevance as it is the N-terminus sequence of human serum albumin (HSA), which is known to chelate Cu^{II} ions at high affinity and is the main Cu^{II} binding protein along with ceruloplasmin and alpha-2-macroglobulin.[35] Such a sequence beginning by a free N-terminal amine and having a His residue at the third position belongs to the broader family of ATCUN (Amino-Terminal Cu and Ni binding) motifs, and DAHK is the prototypical case.[36-37] Such ATCUN motifs have been reported to lessen Cu(Aβ) induced toxicity, and[38-40] some of the N-truncated Aβ peptides (at positions 4 and 11) do themselves exhibit such motif.[26, 39-46] The GHK peptide and its Cu^{II} complex have been extensively studied concerning their biological function. Some of the critical roles of Cu(*H*-1GHK) and GHK include stimulating wound healing and tissue regeneration.[47-50] Similarly to DAHK, Cu^{II} bound to GHK represents a prototypical coordinating family, to which peptides belong when having a His in the second position together with a free N-terminal amine. This motif can be obtained by N-terminal truncation of the Aβ sequence at position 5 and has been shown very recently to interact with Cu(Aβ) and modulate the Cu^{II} homeostasis.[51] The solution structures of Cu(*H*-1GHW) and Cu(*H*-2DAHW) complexes are shown in **Figure 1**. These Trp-containing complexes have the same coordination chemistry as their Cu(*H*-1GHK) and Cu(*H*-2DAHK) counterparts, but with the benefit of having a fluorescent probe sensitive to Cu^{II} binding.[22] Tryptophan (Trp, W) fluorescence is quenched upon the binding of Cu^{II} to the GHW or DAHW.[20-22]

The current work reports on the overall exchange rate from CuAβ complexes to GHW and DAHW, using the interpeptidic Cu^{II} exchange kinetics measurement through a quantitative tryptophan fluorescence quenching method. We will also discuss possible mechanisms and steps of the Cu^{II} exchange based on the review of relevant literature. This discussion will mainly include the variables that affect the rate constant, including the pH, the length of the Aβ peptide, the location of the anchoring histidine ligand in the fluorescent peptide, and the number of amide deprotonations required in the tryptophan peptide to coordinate the Cu^{II}. The importance of Cu^{II} exchange in these peptides is critical to understanding disease mechanisms that rely on metal ion homeostasis that has been implicated in neurological diseases like AD. Accurate measurement of their exchange constants will help to elucidate the complex Cu^{II} homeostasis in the synaptic cleft and blood where so many peptides can compete for binding Cu^{II}.

Experimental Methods

Materials. All peptides were used as purchased from the manufacturer. The GHW (99.73% pure) and DAHW (96.89%) peptides used were purchased from GeneCust (Luxembourg). The $A\beta_{1-16}$ (>95%) and $A\beta_{1-28}$ (>95%) peptides were purchased from Synpeptide Co., Ltd (China). The source of Cu^{II} ions was $CuSO_4 \bullet 5H_2O$ and was purchased from Aldrich. Buffer chemicals HEPES (99.5%) and NaOH (97.0%) were purchased from Sigma. A Synergy Milli-Q purification system purified all water used to 19 MΩ•cm resistivity. ^{65}Cu was obtained from a ^{65}Cu foil from Eurisotop. Quartz cuvettes (Firefly) were used in all absorption and emission spectroscopy with 1 cm path-lengths. All solid peptides were stored in a -20°C freezer.

Instrumentation. Fluorimetry measurements were performed on a Horiba Jobin-Yvon FluoroLog-3 spectrofluorometer. Absorption measurements were performed with an AvaLight DHc dual deuterium-halogen lamps light source for spectroscopy in the 200 – 2500 nm range and AvaSpec-2048 detector. The cuvette holder was attached to the light source and the detector by fiber optic cables. EPR spectra were taken on a Bruker 9 GHz ELEXSYS spectrometer from 2500 G to 3700 G, 0.5 mT amplitude modulation, approximately 9.5 GHz, and at 120 K. Spectra were recorded using a microwave power of 5 mW.

EPR simulations. EPR spectra were simulated by using the Easyspin software package[52] and routines written in the lab. The Cu^{II} centers were defined by their g-values and hyperfine couplings. Superhyperfine couplings with relevant nitrogen nuclei were also included. Anticorrelated g- and A- strains were used on Cu^{II} to better simulate line-broadening observed experimentally. Simulation parameters. Cu(H_{-1}GHW): $g_{//}$=2.235 (g-strain 0.008), $g_{\perp}$=2.052 (g-strain 0.005); $A_{//}$=606MHz (A-strain 20MHz), $A_{\perp}$=46MHz (A-strain 5MHz); 3 equivalent N nuclei with A_N=42 MHz. Cu(H_{-1}GHW)(Im): $g_{//}$=2.209 (g-strain 0.009) $g_{\perp}$=2.052 (g-strain 0.006); $A_{//}$=652MHz (A-strain 20MHz) $A_{\perp}$=46MHz (A-strain 5MHz); 4 equivalent N nuclei with A_N=43 MHz. Weights for simulation of spectrum c : Cu(H_{-1}GHW) 42%, Cu(H_{-1}GHW)(Im) 58%.

Parameters for fluorimetry and UV-vis spectroscopies. Fluorimetry parameters included 1.5 nm excitation and emission slit widths, an excitation wavelength of 290 nm, an emission wavelength of 365 nm, and a 0.25 s time interval (kinetics) with quartz cuvettes ℓ = 1.0 cm. Absorption parameters included a boxcar width of 5 and an average of 100 scans per capture. A thin layer, ℓ = 1.7 mm, quartz cuvette was used. To keep with one unique buffer over the pH range, we used HEPES buffer and checked that no pH changes occurred during the experiments. We calculated that despite the high HEPES buffer concentration compared to the peptide ones (100 mM vs. 4-7 μM, respectively), only 5% of Cu is bound to the buffer in the fluorescence experiments (according to formation constants reported in refs.[3] and [53]).

Stock solution preparation, concentration titrations, and sample preparation. For sample preparation, stock peptide concentrations, Cu(Aβ) solutions, fluorimetry sample preparation, and EPR sample preparation, please see the Supporting Information (SI available free of charge). A daily calibration curve was performed for all fluorescent peptides from 1 – 10 μM in triplicate. Please see the SI for software used and detailed information on the stock peptide concentration determination, creation of Cu(Aβ) complex solution for kinetic experiments, how the Trp-containing peptide was calibrated in the fluorescence experiments, and kinetic fluorescence sample preparation.

Results

Cu^{II}-peptide coordination. The Cu^{II} coordination to GHW and DAHW has been reported.[22] In **Figure 2 and Table 1,** we list the EPR signatures and parameters of the Cu(H_{-1}GHW) and Cu(H_{-2}DAHW) complexes. They perfectly agree with the previous report[22] and will serve for a direct comparison with Cu(Aβ) and species resulting from the Cu^{II} exchange. The EPR signatures of the starting $Cu(A\beta_{1-16})_I$ and $Cu(A\beta_{1-16})_{II}$ complexes were recorded under the same conditions and are reported as a reference. The classical fingerprint where the EPR signatures of components I and II superimpose in an approximately 80/20 (I/II) ratio is obtained.[30-31, 54-55]

Table 1: Experimental EPR constants of all Cu^{II} peptide complexes studied and discussed.

Complex	$g_{//}$	$g_{\perp}$	$A_{//}(^{65}Cu)$ MHz
Cu(H_{-1}GHW)[22,[a]]	2.23	2.05	560
Cu(H_{-1}GHW)[22,[a]] simulation	2.24	2.05	606
Cu(H_{-2}DAHW)[22]	2.18	2.05	588
$(CuA\beta_{1-16})_I$ [54[b]]	2.26	2.06	580
$(CuA\beta_{1-16})_{II}$ [54[b]]	2.23	2.05	520
Cu(H_{-1}GHW)(Im) simulation	2.21	2.05	652

[a]Obtained with $^{63/65}Cu$ mixture in natural isotopic abundance. [b] obtained with ^{63}Cu and corrected to be directly comparable with ^{65}Cu spectra.

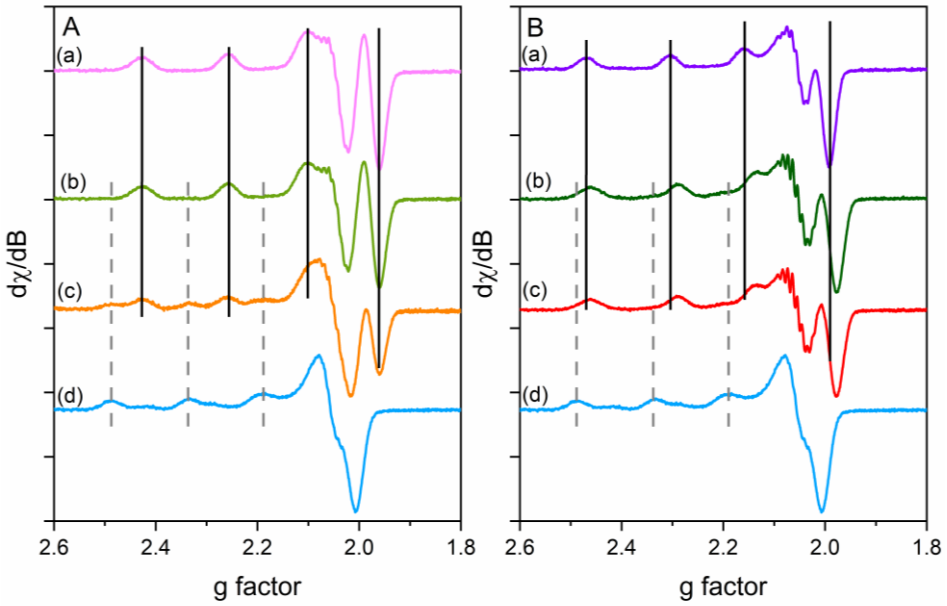

Figure 2: The low temperature (120 K) X-band EPR spectra of Cu(H_{-2}DAHW) (panel A, line a, lilac) and Cu(H_{-1}GHW) (panel B, line a, purple) controls, the reaction of Cu($A\beta_{1\text{-}16}$) and DAHW or GHW at 1.0 mol equivalence and frozen at 5 minutes after mixing to reach an equilibrium (panels A and B, lines b, green), of Cu($A\beta_{1\text{-}16}$) and DAHW or GHW at 1.0 mol equivalence and frozen as soon as possible (asap) upon mixing (panels A and B, lines c, orange and red), and of the Cu($A\beta_{1\text{-}16}$) control (panels A and B, line d, blue). The solid vertical lines follow the first three parallel transitions for Cu(H_{-2}DAHW) (panel A) and Cu(H_{-1}GHW) (panel B) and for Cu($A\beta_{1\text{-}16}$) are the dashed lines. Experimental conditions [^{65}Cu] = 450 μM, [GHW] = [DAHW] = [Aβ] = 500 μM. [HEPES] = 100 mM, pH 7.4. 10% of glycerol was used as a cryoprotectant.

Cu^{II} interpeptidic exchange kinetics. Using the same fluorimetry methodology as we previously published on the interpeptidic exchange between Cu(H_{-1}GHW) to GHK and DAHK,[22] we monitored the complete exchange of Cu^{II} from Cu($A\beta_{1\text{-}16}$) and Cu($A\beta_{1\text{-}28}$) to the fluorescent Trp-containing peptides P (GHW or DAHW) at three pHs 6.8, 7.4, and 8.7 in 0.1 M HEPES. The exchange follows **Eq. 1**, where *b* and *n* are the number of deprotonated amide N^- in the Cu(H_{-b}Aβ) and Cu(H_{-n}P) complexes. Deprotonations at the N-terminus (pKa > 8), amide backbone NH (pKa > 14), and His residues (pKa ≈ 6-7) must occur for the Trp-containing peptide to coordinate Cu^{II}. These deprotonations are determined by pH and the prior anchoring of Cu^{II} in the coordinating group's vicinity, decreasing the effective pKa value by chelate effects.[7]

$$(\mathbf{1})\ Cu(H_{-b}A\beta) + P \longrightarrow Cu(H_{-n}P) + A\beta + (n-b)H^+$$

The two peptide complexes created upon the exchange from Cu(Aβ) are Cu(H_{-1}GHW) and Cu(H_{-2}DAHW), and their overall charges are omitted for clarity. Note that the possibility of making the ternary complex Cu(H_{-1}GHW)(N_{im})$_{A\beta}$ is omitted here for simplicity but will be discussed later. Since the Cu(Aβ) complex has a predominant form at pH 6.8 (Cu(Aβ)$_I$) and at pH 8.7 (Cu(Aβ)$_{II}$), which are in equilibrium at pH 7.4, we measured the interpeptidic Cu^{II} exchanges at all three pHs.

The kinetic data were fit using a second-order rate expression shown in **Eq. 2**, where initial concentrations are denoted with a subscript 0, and the variable concentration is represented with a subscript t. The rate constant, *k*, is determined by the slope when the y-intercept is set through the origin. Since the variable [Cu(Aβ)]$_t$ is unknown, we must estimate it. The exchanged [Cu^{II}] can be determined by the amount of diminished Trp peptide (P) (P = GHW, DAHW) fluorescence (assuming all peptides coordinate in a 1:1 ratio under the experimental conditions) and the initial [Cu(Aβ)]$_0$ (determined from the stock Cu^{II} and Aβ solutions). Therefore, the [Cu(Aβ)]$_t$ equals [Cu(Aβ)]$_0$ minus the change in concentration of the fluorescent peptide **Eq. 3**. These reactions go to near completion in the GHW and DAHW exchanges due to the three orders of magnitude larger association constants. The **Eq. 2** y value is denoted as y(P) in the figures where P = GHW, or DAHW.

$$(2)\ ([Cu(A\beta)]_0 - [P]_0)^{-1} * \ln\left(\frac{[P]_0 * [Cu(A\beta)]_t}{[Cu(A\beta)]_0 [P]_t}\right) = k * t$$

$$(3)\ [Cu(A\beta)]_t = [Cu(A\beta)]_0 - ([P]_0 - [P]_t)$$

There are sources of uncertainty in both starting concentrations for $[Cu(A\beta)]_0$ and $[P]_0$ that can make the linear regression line deviate from a natural y-intercept through the origin. We estimate that the uncertainty in the rate constant due to the error in concentration is about 6 - 9%. Most of the uncertainty in starting concentrations lies in the determination of $[Cu(A\beta)]_0$ since there is no way to spectroscopically measure this, unlike for the fluorescent peptides (P). For [P] determination, a daily calibration is done, and the initial data point $[P]_0$ can be measured with a known uncertainty of about 2-4%. The other 4-5% comes from propagated errors in the determination of $[Cu(A\beta)]_0$ based on the independent determination of the [Aβ] and [Cu^{II}] stock solutions by UV-vis, errors in the volume of each added to create $[Cu(A\beta)]_{stock}$, and the volume error when diluting within the cuvette.

It is notable to mention that the measurement of kinetic rate constants is usually performed under pseudo-first-order conditions where one reactant is in a large excess of the other. With metal ion peptide complexes, such conditions will change speciation and can induce complexes to form where multiple peptides coordinate to the metal.[56-57] To avoid this, we chose to use similar reactant concentrations with no large excesses. Specifically, the reaction concentrations were within 1-2 μM of each other, such as in 4 μM GHW + 5 μM Cu(Aβ$_{1-16}$). The tryptophan peptides ranged from 4 – 6 μM, and the Cu(Aβ) complexes ranged from 4 – 7 μM. The experimentally obtained initial concentrations of both Cu(Aβ) complexes and peptides are given in **Table S1** along with the slopes and R^2 values from the fitting using **Eqs. 2-3**.

A typical kinetic trace (*inset*) and second-order fit of the data which has been transformed using **Eq. 2/3** is shown in **Figure 3**, where the 4 μM P + 5 μM Cu(Aβ$_{1-16}$) concentration profile is shown for when P = GHW (A) and DAHW (B) for pH 7.4. The kinetic data were manually inspected to determine what time the plots began to plateau. So, depending on the exchange complex formed, the data used to determine the rate constant is anywhere from the first 9 – 18 s for the GHW or DAHW exchanges, **Table S1**. Each concentration profile was run in triplicate so that 11-15 individual rate constants were measured for each exchange process, **Table S1**. These second-order rate constants were then averaged and are reported here with 95 % confidence, **Table 2.** We include our previously measured rate constants for comparison.[22] We have also added the reverse exchange constant for the Cu(*H*$_{-1}$GHK) + GHW reaction to facilitate our discussion on the importance of the releasing peptide. Detailed information on this exchange is available in the SI section 3.

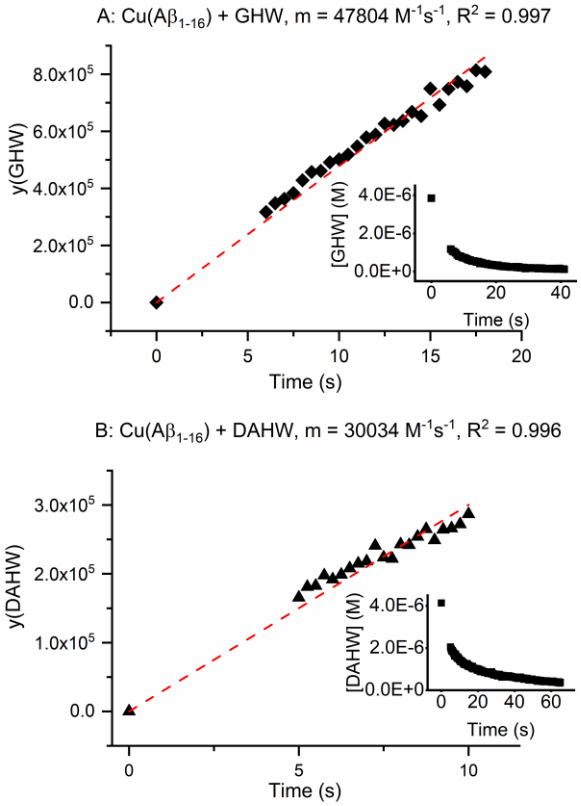

Figure 3: Kinetic data transformed by second-order fitting for the 4 μM P + 5 μM Cu(Aβ$_{1-16}$) exchanges (approximate concentration) at pH 7.4 in 0.1 M HEPES buffer when P = GHW (A) and DAHW (B). The y-axis is the y-value in (**Eq. 2+3**), and the x-axis is time (s). Which peptide the Cu^{II} is forming a complex with is denoted by y(P). Insets are the kinetic data in concentration (M) versus time (s).

Table 2: Conditional second-order rate constants between P + Cu(Aβ) and Cu(*H*$_{-1}$GHK) exchanges in 0.1 M HEPES at confidence levels of 95%. The previous rate constants reported for exchange from Cu(*H*$_{-1}$GHW) to GHK or DAHK are also listed.[22]

	k_P (x 10^4 $M^{-1}s^{-1}$)		
Exchange	pH 6.8	pH 7.4	pH 8.7
Cu(Aβ$_{1-16}$) + GHW	4.3±0.3	4.4±0.3	3.0± 0.3
Cu(Aβ$_{1-28}$) + GHW	1.73±0.08	2.83±0.19	1.22±0.15
Cu(Aβ$_{1-16}$) + DAHW	1.51±0.11	2.84±0.15	2.48±0.19
Cu(Aβ$_{1-28}$) + DAHW	0.81±0.08	1.95±0.13	1.32±0.17

Cu(*H-1*GHW) + GHK [22]	0.016±0.002
Cu(*H-1*GHK) + GHW	0.043±0.003
Cu(*H-1*GHW) + DAHK [22]	0.0050±0.0007

In **Figure 2**, we report the EPR signatures of the species present after mixing Cu(Aβ$_{1-16}$) with GHW or DAHW and freezing as soon as possible (asap, orange and red lines, c) and after reaction completion (time 5 minutes, green lines, b). For the DAHW peptide immediately frozen upon mixing, the EPR fingerprint (panel A, c) is made of two components corresponding to Cu(Aβ$_{1-16}$) and Cu(*H-2*DAHW) (as indicated by the vertical lines) in approximately 40/60 ratio (Cu(Aβ$_{1-16}$)/Cu(*H-2*DAHW)). At the end of the reaction (panel A, b), all of the Cu^{II} has been exchanged to the DAHW peptide creating only Cu(*H-2*DAHW) as the EPR spectrum is identical to the Cu(*H-2*DAHW) control (panel A, a). This result is in line with fluorescence measurements and respective affinities of both peptides.[3, 36]

For GHW, the EPR fingerprint obtained and shown in **Figure 2** is almost the same regardless of whether the solution was frozen immediately (asap, panel B, c) or after waiting 5 minutes to achieve equilibrium (panel B, b). In the asap spectrum (panel B, c), there is only a remaining weak contribution of Cu(Aβ$_{1-16}$) signature (<10%), while after completion (panel B, b), the amount of Cu(Aβ$_{1-16}$) is about 5%. These differences indicate that equilibrium in the GHW exchange is reached faster than with DAHW, in accord with the kinetic fluorescence data. The EPR fingerprint obtained for mixing Cu(Aβ$_{1-16}$) and GHW is different from those obtained for control spectra of Cu(Aβ$_{1-16}$) and Cu(*H-1*GHW) and does not correspond to a simple combination of these two signatures as observed for DAHW. The EPR spectrum is strongly reminiscent of ternary species, where the Cu^{II} is predominately coordinated to the GHW peptide, and the fourth equatorial position is occupied by an imidazole ring of another His containing peptide instead of a coordinated water molecule.[24]

We performed additional EPR simulation experiments of the key spectra to check the nature of the ternary species formed between Cu(Aβ) and GHW, **Figure 4**. The EPR signature of Cu^{II} bound to GHW in the presence of one and three equivalents of imidazole (Im) (to model the three His in the Aβ sequence) are shown in **Figure 4** (c and b, respectively). The resulting spectra are virtually identical to that of Cu(Aβ) + GHW (compare spectra (b) and (c) in **Figure 4**). In addition, we also performed the EPR simulation of the Cu(*H-1*GHW) spectra (in the absence or presence of one equiv. Im). The values obtained are listed in **Table 1**. Of interest is the need to include two components in a 42/58 ratio to simulate the Cu(*H-1*GHW) + 1 equiv. Im spectrum. The first component corresponds to Cu(*H-1*GHW), and the second one is attributed to the 4N species Cu(*H-1*GHW)(Im) (spectrum d). The EPR parameters fully agree with a 4N coordination according to the Peisach and Blumberg correlation.[58-59] While EPR observes this ternary species at a working concentration of 0.5 mM; it must be noted that it may not be predominant under the fluorescence experiments working concentration of approximately 5 μM. Based on values reported for the formation of ternary species similar to Cu(*H-1*GHW)(Im),[50] we found that about 50% of ternary species are formed at 0.5 mM, in perfect agreement with the 42/58 Cu(*H-1*GHW)/Cu(*H-1*GHW)(Im) ratio found here. In comparison, less than 1% is formed at the fluorescence concentration of 5 μM. Taken together, this indicates that the Cu^{II} has been completely extracted from Aβ by the GHW in the fluorescence experiments, creating a larger population of Cu(*H-1*GHW) at the μM concentrations. In contrast, the EPR experiments performed at 0.5 mM concentrations resulted in the Cu(*H-1*GHW) and the ternary species Cu(*H-1*GHW)(N$_{im}$)$_{Aβ}$ in a 42/58 ratio. The structure of Cu(*H-1*GHW)(N$_{im}$)$_{Aβ}$ has the fourth position around the Cu^{II} occupied by one of the His imidazole group from Aβ instead of the water molecule initially present (**Figure 1**).

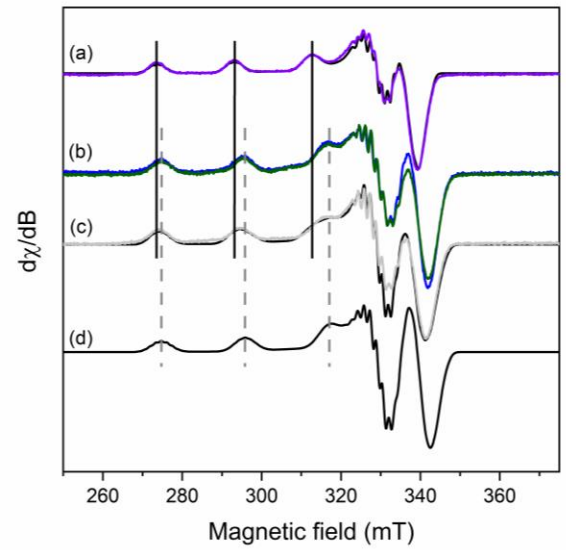

Figure 4: The low temperature (120 K) X-band EPR spectra of Cu(*H-1*GHW) (line a, purple) and its simulated spectrum (line a, black), of Cu(Aβ$_{1-16}$) and GHW at 1.0 mol equiv. at equilibrium (line b, green), of Cu(*H-1*GHW) in the presence of 3 equiv. of Im (line

b, blue), of Cu(H_{-1}GHW) in the presence of 1 equiv. of Im (line c, grey) and its simulated spectrum (line c, black), and the theoretical spectrum corresponding to the 4N species Cu(H_{-1}GHW)(Im) (line d). The solid vertical lines follow the first three parallel transitions for Cu(H_{-1}GHW), and the dashed vertical lines follow the parallel transitions for Cu(H_{-1}GHW)(Im). Experimental conditions [^{65}Cu] = 450 μM, [GHW] = [DAHW] = [Aβ] = 500 μM, [Im] = 500 μM or 1500 μM, [HEPES] = 100 mM, at pH 7.4 with 10% of glycerol as a cryoprotectant.

Discussion

Two possible interpeptidic Cu^{II} exchange pathways can be envisioned: an associative or dissociative pathway (**Scheme 1**). In the associative pathway, the Cu^{II} is exchanged from Cu(Aβ) to the Trp-containing peptide (P) via the formation of a transient ternary species (Cu(Aβ)(P)). In our previous work, the exchanges of Cu^{II} from Cu(H_{-1}GHW) to GHK and DAHK peptides depended on forming such a ternary species.[22] In the dissociative pathway, Cu^{II} has to first dissociate from Cu(Aβ) and then be captured by DAHW or GHW. This dissociative mechanism was ruled out in the case of exchange between Cu(H_{-1}GHW) to GHK and DAHK due to the unfavored and extremely slow dissociation of Cu^{II} from the Cu(H_{-1}GHW) complex.[22] However, this is not the case when the releasing peptide is Aβ because the dissociation of Cu^{II} from Cu(Aβ) lies on the ms time scale.[60-61] With the methodology used here, we can not discriminate between the two pathways. However, the various trends observed on the rate constants as a function of pH, releasing peptide, receiving peptide, and so on can be discussed in light of the available literature regardless of the pathway followed. A more detailed sequential analysis of each pathway is proposed in **Scheme 2**.

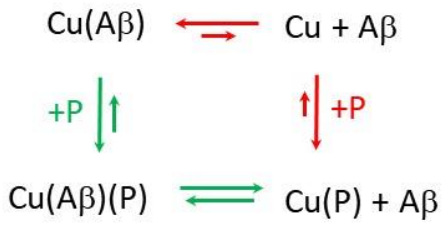

Scheme 1: Schematic to represent dissociative (red) versus associative (green) pathways for Cu^{II} exchange from Aβ. P indicates the receiving Trp-containing peptide.

Proposed reactions in the interpeptidic Cu^{II} exchange based on experimental data and literature. We propose the following reactions for the exchange of Cu^{II} between Cu(Aβ) complexes to the small Trp-containing peptides (**Scheme 2**). The double arrows denote equilibrium processes, and larger forward reaction arrows indicate thermodynamic favorability in that direction. There are various reactions at play in the interpeptidic Cu^{II} exchange observed here, which have relevance in the literature and must be discussed, **Scheme 2**.

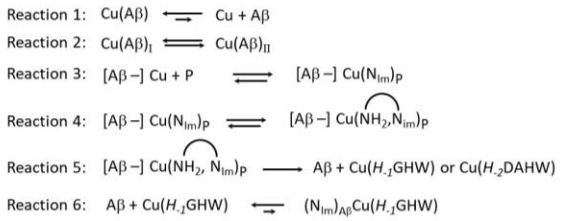

Scheme 2. Cu^{II} exchange between Cu(Aβ) complexes and the small peptides GHW and DAHW (denoted as P). The arrows show equilibrium processes, and weights in direction are based on thermodynamic favorability (at the fluorescence concentration). (NH_2,N_{im}) indicates the formation of a metallacycle between the N-terminal amine and the imidazole side chain of His.

(i) Reaction 1 is the equilibrium corresponding to Cu(Aβ) dissociation and Cu^{II} + Aβ association. Reaction 1 is driven by the affinity value of Cu^{II} for Aβ in the working conditions, which equals about 10^7 M^{-1} here. This value is obtained from the affinity at pH 7.4 (about 10^{10} M^{-1})[3] corrected for the competition with 0.1 M HEPES buffer.[53] The k_{off} value reported in the literature lies between 0.1 s^{-1} and 0.8 s^{-1}.[60-61] This rate is fast enough to consider the possibility of having a dissociative pathway.

(ii) Reaction 2 is the equilibrated interconversion of $Cu(Aβ)_{II}$ to $Cu(Aβ)_I$ and will be more influential at pH 7.4 and 8.7 but not at pH 6.8 where most species are present as $Cu(Aβ)_I$.[7-8, 60] Note that according to the report by Ying et al.,[60] $Cu(Aβ)_I$ must form for subsequent reactions to follow. Since the GHW and DAHW Cu^{II} exchanges go to completion, then the $Cu(Aβ)_{II}$ is thermodynamically favored to convert to $Cu(Aβ)_I$. The $Cu(Aβ)_{II}$ is obtained by deprotonation and binding of an amide NH from $Cu(Aβ)_I$ and concomitant departure of one His imidazole ligand. It has been reported that the interconversion rate constants for $Cu(Aβ)_I$ to $Cu(Aβ)_{II}$ is 1.5 s^{-1} and for $Cu(Aβ)_{II}$ to $Cu(Aβ)_I$ is 2.5 s^{-1}.[60] This interconversion reaction may be significant in our studies as all Cu^{II} is exchanged from $Cu(Aβ)_I$ and thus, to remove Cu^{II} from $Cu(Aβ)_{II}$, it must be first converted to $Cu(Aβ)_I$.[60]

(iii) Reaction 3 is the Cu^{II} anchoring site from either Cu(Aβ) or Aβ-unbound Cu^{II} (both regrouped under the notation [Aβ—] Cu) by the incoming peptide GHW or DAHW. Based on literature and pKa of the various anchors[62], the Cu^{II} is coordinated to the small peptides in a monodentate manner through a His residue (via the imidazole ring, noted N_{Im}).[62]

(iv) After anchoring via the His residues, reaction 4 corresponds to creating a metallacycle between the His and the second anchor, the N-terminal amine. GHW and DAHW follow ATCUN intermediate species pathways described by Kotuniak et al., where these two sites coordinate before the amide backbone N^-.[63]

(v) Then reaction 5 concerns the deprotonation and subsequent binding of the amide bond(s) in between the two nitrogen anchors leading to the 3N (GHW) or 4N (DAHW) main binding sites (shown in **Figure 1**). The binding of amide N leads to the formation of stable adjacent 5 or 6 membered metallacycles between the Cu^{II} and the Trp-containing peptides. The amide deprotonations and coordination result in the complete exchange of Cu^{II} to the final species, Cu(*H*$_{-2}$DAHW) or Cu(*H*$_{-1}$GHW), and releases the Aβ peptide.

(vi) In the case of GHW, the ternary Cu(*H*$_{-1}$GHW)$(N_{im})_{Aβ}$ species can form depending on the working concentrations (reaction 6).

It is worth noting here that a partial quenching may be obtained even if Cu(*H*$_{-1}$GHW) and Cu(*H*$_{-2}$DAHW) complexes are not formed, provided that the Trp is close enough to the Cu^{II} center (within 14 angstroms) in the intermediate complexes (reactions 3-5). In contrast, a complete quenching of the Trp fluorescence can only be achieved once these final species are formed. However, considering that reaction 3 is extremely fast[63] and that we could not record the first 4-5 seconds of the kinetic experiments, the reactions 1, 2, and 4-6 are probed here. The variations observed in the overall exchange rate constants (**Table 2**) are consistent with the sequence of reactions proposed in **Scheme 2.** This is discussed below, along with several key variables that affect the observed rate constant.

Cu^{II} Exchange from Small Peptides versus Amyloids. Previously we examined the interpeptidic exchange of Cu^{II} from Cu(*H*$_{-1}$GHW) to GHK and DAHK.[22] To directly compare Cu^{II} removal from Cu(Aβ) and the Trp-containing complexes, we investigated the reverse exchange constant of Cu(*H*$_{-1}$GHK) to GHW and determined k_{GHW} = 4.3(± 0.3) x 10^2 $M^{-1}s^{-1}$ using the previously described method (See the SI section 3 for a detailed analysis).[22] Note that the value determined here for Cu^{II} removal from Cu(*H*$_{-1}$GHK) (by GHW) is on the same order of magnitude as the removal determined from Cu(*H*$_{-1}$GHW) (by GHK).[22] The 2.5 fold increase may be related to the slightly larger affinity of GHW (versus GHK) for Cu^{II}, as postulated in our previous work.[22] The Cu^{II} exchange rate constants are larger by 2 – 3 orders of magnitude when Cu^{II} is exchanged from the Cu(Aβ) rather than from the Cu(*H*$_{-1}$GHK) or Cu(*H*$_{-1}$GHW) to the GHW/GHK or DAHK peptides at pH 7.4, **Table 2**.

In our previous paper,[22] we discussed that the exchange between the Cu(*H*$_{-1}$GHW) to GHK or DAHK peptides proceeded via the formation of a ternary species, where the receiving peptide likely binds first through the N_{im} from the His residue. The reverse exchange Cu(*H*$_{-1}$GHK) + GHW reported here has a rate constant on the same order of magnitude as the forward exchange previously measured. Looking collectively at both directions of the Cu^{II} exchange between GHK/GHW indicates that the Cu^{II} dissociation from the GHK/W peptide is far too weak to fuel a dissociative mechanism; thus, an associative mechanism is more likely to occur. With Aβ, Cu^{II} dissociation is more favored than with GHK/W since the affinity of Cu^{II} for Aβ is three orders of magnitude weaker than those for GHK/W.[3, 50] As a consequence, the significantly large difference in exchange rates between Cu^{II} removal by GHW from Aβ or GHK (i) indicate the contribution of a dissociative mechanism in the case of Aβ, and/or (ii) agree with the fact that in reactions 4-5, the formation of metallacycles within the receiving peptide P is a driving force that is significantly lessened when similar adjacent metallacycles are already present in the starting Cu^{II}-complex.

Importance of the receiving Trp-containing peptide sequence in exchange from Cu(Aβ) complexes. The GHW exchanges are always faster than the DAHW exchanges, except with Cu($Aβ_{1-28}$) at pH 8.7, where they are statistically similar. This trend is likely due to the combination of effects. The Cu(*H*$_{-1}$GHW) complex requires only one amide deprotonation, forming two adjacent metallacycles, and has a coordinated water molecule. In comparison, the Cu(*H*$_{-2}$DAHW) complex requires two amide deprotonations to create three adjacent metallacycles and has no coordinated water. The higher the pH, amide deprotonations become easier to accommodate the Cu^{II}. Chelate effects effectively lower the pKa of these motifs. Thus, NH_3^+ deprotonations become a more critical variable on the measured rate constant than the amide N^- deprotonations.[25, 63] It can be anticipated that the formation of a larger metallacycle in Cu(*H*$_{-2}$DAHW) versus in Cu(*H*$_{-1}$GHW) created between the anchoring His N_{im} and the N-terminal amine in the intermediate 2N species (reaction 4, **Scheme 2**) is less favored.

Also, the presence of a bulky residue at the N-terminus may deter Cu^{II} binding there compared to the Gly residues' hydrogen side-chain. Combined, these effects slow down the rearrangement of the Cu^{II} coordination sphere to a larger extent for DAHW than for GHW and are one consideration as to why we observe faster exchange rates for GHW.

The Effect on the Rate Constant Due to Aβ length. In **Table 2,** all of the Cu($Aβ_{1-16}$) exchanges to GHW and DAHW at each pH had larger rate constants than the corresponding Cu($Aβ_{1-28}$) exchanges. For the GHW exchanges, the Cu($Aβ_{1-16}$) rate constants are 1.6 (pH 7.4) or 2.5 (pH 6.8 and 8.7) times faster than the corresponding Cu($Aβ_{1-28}$) exchanges. Similarly, for DAHW, these are 1.5 (pH 7.4) or 1.9 (pH 6.8 and 8.7) times faster for Cu($Aβ_{1-16}$) than Cu($Aβ_{1-28}$). Since the $Aβ_{1-28}$ peptide has more aliphatic residues surrounding the Cu^{II} coordination sphere, this presents a physical barrier to the Trp-containing peptide's initial coordination to the Cu^{II} by a N_{im} in the GHW/DAHW (reaction 3, **Scheme 2**). This physical impedance would result in a slower formation of the $Aβ(Cu)(N_{im})_P$ ternary species for the Cu($Aβ_{1-28}$) complex than for Cu($Aβ_{1-16}$). This argument works for the associative pathway contribution to the overall exchange mechanism. For the dissociative pathway, the trend observed is in line with an equilibrium between Aβ-bound or Aβ-unbound Cu^{II} that is more displaced towards Aβ-bound in the case of the $Aβ_{1-28}$ as the Cu^{II} affinity is higher for $Aβ_{1-28}$ compared to $Aβ_{1-16}$.[32, 64]

Importance of pH effects. The trend observed as a function of pH has a bell-shape with the highest rate observed at pH 7.4, where the two Cu(Aβ) components are in equilibrium. This agrees with a combination of two opposite effects: (i) the interconversion from $Cu(Aβ)_{II}$ to $Cu(Aβ)_I$ on observed rate constants and (ii) the protonation state of His from the receiving peptide. (i) The exchange of Cu^{II} from the Cu(Aβ) complex is dependent on the form as exchange happens from $Cu(Aβ)_I$, reaction 2, **Scheme 2**. At pH 6.8, all species are $Cu(Aβ)_I$ before the addition of the Trp peptide, so there is no effect on the whole kinetic reaction at this pH for the GHW and DAHW exchanges. For the other two pH values, as the pH increases, the proportion of $Cu(Aβ)_I$ decreases while the proportion of $Cu(Aβ)_{II}$ increases. At pH 7.4, 20% of the species are now $Cu(Aβ)_{II}$ (before adding P), and at pH 8.7, >90% of species are $Cu(Aβ)_{II}$. If the rate constants were only affected by this pH effect of the interconversion of Cu(Aβ), we would have expected a decrease in the rate constant with the pH increases, as more species would be $Cu(Aβ)_{II}$ as pH increased and need to be converted to $Cu(Aβ)_I$ before the exchange reaction occurs. (ii) In fact, this effect is balanced by another one, the protonation state of His from the receiving Trp-containing peptide. A deprotonated His will more easily anchor the Cu^{II} than one that is protonated. The pKa of His in GHW and DAHW peptides are both about 6.5 based on pKa values of their GHK and DAHK counterparts. .[63, 65-66]

Conclusions

We have measured the interpeptidic Cu^{II} exchange rate constants from Cu(Aβ) complexes to the tryptophan-containing GHW and DAHW using our modified quantitative fluorescence quenching method. The interpeptidic Cu^{II} exchange rate constants are on the order of magnitude of 10^4 $M^{-1}s^{-1}$. We discussed many variables that contribute to the observed rate constants. These variables include the pH value, the length of the Aβ peptide, the number of amide deprotonations needed in the tryptophan peptide to coordinate the Cu^{II}, the interconversion of Cu(Aβ) components, and the extent of metallacycles formed in the Cu(H_{-n}P) complexes. The rate-limiting steps are a combination of all these effects. The six reactions shown in **Scheme 2** affect the rate constants by different magnitudes and influence the overall mechanism by the variables described above.

The homeostasis of metal ions that exist in the brain is vital to the development of neurodegenerative disease. Especially those diseases in which peptides coordinate these metals, like in Alzheimer's disease. These studies provide important insights for the measurement of interpeptidic exchange rates of Cu^{II} between Cu(Aβ) complexes with other peptide motifs, including N-truncated Aβ.[26, 51] With advances in the field, Cu^{II} exchange to and from full-length Aβ peptides in both their soluble monomeric or insoluble aggregated forms can be investigated, as these are the more common biologically relevant forms found in AD pathology. Only a handful of kinetics studies have been reported so far on the Cu^{II} exchange of biological interest.[22, 46, 63] For instance, those studies in which peptides or model peptides can mimic species found within the synaptic cleft where AD occurs. Indeed, the current regard for the peptides studied provides mainly static and conditional kinetic information. However, this thermodynamic view of our obtained data is only a piece of the whole puzzle that additional kinetic insights should complete.

ASSOCIATED CONTENT

Supporting Information. (SI) This material is available free of charge via the Internet at http://pubs.acs.org. The SI includes detailed experimental methods, tables of kinetic data, and information on the reverse exchange between GHW and GHK.

AUTHOR INFORMATION

Corresponding Authors

* Christelle Hureau (christelle.hureau@lcc-toulouse.fr)
* Debbie C. Crans (Debbie.Crans@colostate.edu)

Author Contributions

Authors CNB, DCC, and CH contributed to the conception, editing, and writing of the work. LJZ aided in the collection of data. CNB performed all the fluorescence data analysis and conferred with DCC/CH. KPM, CE, CH, and PD completed the EPR studies. CE and CNB participated in the editing of the revised version. All authors have given their approval to the final version of the manuscript.

Funding Sources

CH, KPM, and CE acknowledge funding from the ERC StG-638712 "aLzINK" grant. CNB and DCC thank the ACS Petroleum Research Fund through grant 55242-ND6. We thank the Chateaubriand Fellowship for the 2015 support of CNB, which fostered this collaboration.

ORCID

Cheryle N. Beuning 0000-0002-3990-6075
Luca Zocchi 0000-0001-9649-2764
Pierre Dorlet 0000-0001-7394-3374
Debbie C. Crans 0000-0001-7792-3450
Christelle Hureau 0000-0003-3339-0239
Kyangwi P. Malikidogo 0000-0002-3556-8283

ACKNOWLEDGMENT

We would like to thank Dr. Michael Johnson and Dr. Nancy Levinger for useful discussions on kinetics. CH, KPM and, CE acknowledge ERC StG-638712 “aLzINK” for financial support. CNB would like to thank Cameron Van Cleave, Allison Haase, and Kateryna Kostenkova for helping her with control experiment data collection at CSU as CNB was no longer an attending student and had since graduated.

REFERENCES

1. Glenner, G. G.; Wong, C. W., Alzheimer's Disease: Initial Report of the Purification and Characterization of a Novel Cerebrovascular Amyloid Protein. *Biochem. Biophys. Res. Commun.* **1984,** *120* (3), 885-890.
2. Wong, C. W.; Quaranta, V.; Glenner, G. G., Neuritic Plaques and Cerebrovascular Amyloid in Alzheimer Disease are Antigenically Related. *Proc. Natl. Acad. Sci. U. S. A.* **1985,** *82* (24), 8729-8732.
3. Alies, B.; Hureau, C.; Faller, P., The Role of Metal Ions in Amyloid Formation: General Principles from Model Peptides. *Metallomics* **2013,** *5* (3), 183-192.
4. Chen, G.-f.; Xu, T.-h.; Yan, Y.; Zhou, Y.-r.; Jiang, Y.; Melcher, K.; Xu, H. E., Amyloid Beta: Structure, Biology and Structure-based Therapeutic Development. *Acta Pharmacol. Sin.* **2017,** *38* (9), 1205-1235.
5. Faller, P.; Hureau, C.; Berthoumieu, O., Role of Metal Ions in the Self-assembly of the Alzheimer’s Amyloid-β Peptide. *Inorg. Chem.* **2013,** *52* (21), 12193-12206.
6. Greenwald, J.; Riek, R., Biology of Amyloid: Structure, Function, and Regulation. *Structure* **2010,** *18* (10), 1244-1260.
7. Chassaing, S.; Collin, F.; Dorlet, P.; Hureau, C.; Gout, J.; Faller, P., Copper and heme-mediated Abeta toxicity: redox chemistry, Abeta oxidations and anti-ROS compounds. *Current topics in medicinal chemistry* **2012,** *12* (22), 2573-2595.
8. Hureau, C.; Dorlet, P., Coordination of redox active metal ions to the amyloid precursor protein and to amyloid-β peptides involved in Alzheimer disease. Part 2: Dependence of Cu(II) binding sites with Aβ sequences. *Coordination Chemistry Reviews* **2012,** *256* (19–20), 2175-2187.
9. Kepp, K. P., Alzheimer’s Disease: How Metal Ions Define β-amyloid Function. *Coord. Chem. Rev.* **2017,** *351* (Supplement C), 127-159.
10. Lovell, M. A.; Robertson, J. D.; Teesdale, W. J.; Campbell, J. L.; Markesbery, W. R., Copper, Iron and Zinc in Alzheimer's Disease Senile Plaques. *J. Neurol. Sci.* **1998,** *158* (1), 47-52.
11. Miura, T.; Suzuki, K.; Kohata, N.; Takeuchi, H., Metal Binding Modes of Alzheimer's Amyloid β-Peptide in Insoluble Aggregates and Soluble Complexes. *Biochemistry* **2000,** *39* (23), 7024-7031.
12. Parthasarathy, S.; Long, F.; Miller, Y.; Xiao, Y.; McElheny, D.; Thurber, K.; Ma, B.; Nussinov, R.; Ishii, Y., Molecular-Level Examination of Cu2+ Binding Structure for Amyloid Fibrils of 40-Residue Alzheimer’s β by Solid-State NMR Spectroscopy. *Journal of the American Chemical Society* **2011,** *133* (10), 3390-3400.
13. Nguyen, M.; Robert, A.; Sournia-Saquet, A.; Vendier, L.; Meunier, B., Characterization of New Specific Copper Chelators as Potential Drugs for the Treatment of Alzheimer’s Disease. *Chemistry – A European Journal* **2014,** *20* (22), 6771-6785.
14. Jomova, K.; Vondrakova, D.; Lawson, M.; Valko, M., Metals, Oxidative Stress and Neurodegenerative Disorders. *Mol. Cell. Biochem.* **2010,** *345* (1), 91-104.
15. Jiang, D.; Zhang, L.; Grant, G. P. G.; Dudzik, C. G.; Chen, S.; Patel, S.; Hao, Y.; Millhauser, G. L.; Zhou, F., The Elevated Copper Binding Strength of Amyloid-β Aggregates Allows the Sequestration of Copper from Albumin: A Pathway to Accumulation of Copper in Senile Plaques. *Biochemistry* **2013,** *52* (3), 547-556.
16. Linder, M. C., Lomeli, N.A., Donley, S., Mehrbod, P.C, Cotton, S., Wooten, L., Copper Transport in Mammals. *Adv. Exp. Med. Biol.* **1999,** *448*, 1-16.
17. Festa, R. A.; Thiele, D. J., Copper: An Essential Metal in Biology. *Curr Biol* **2011,** *21* (21), R877-R883.
18. Waggoner, D. J.; Bartnikas, T. B.; Gitlin, J. D., The Role of Copper in Neurodegenerative Disease. *Neurobiol. Dis.* **1999,** *6* (4), 221-230.
19. Sigel, A. S., H. Sigel R. , *Interrelations Between Essential Metal Ions and Human Diseases*. Springer: Dordrecht, The Netherlands, 2013; Vol. 13, p 1-29, 229-286, 359-381, 389-409.
20. Lehrer, S. S., Fluorescence and Absorption Studies of the Binding of Copper and Iron to Transferrin. *J. Biol. Chem.* **1969,** *244* (13), 3613-3617.
21. Ghisaidoobe, A.; Chung, S., Intrinsic Tryptophan Fluorescence in the Detection and Analysis of Proteins: A Focus on Förster Resonance Energy Transfer Techniques. *Int. J. Mol. Sci.* **2014,** *15* (12), 22518.
22. Beuning, C. N.; Mestre-Voegtlé, B.; Faller, P.; Hureau, C.; Crans, D. C., Measurement of Interpeptidic Cu(II) Exchange Rate Constants by Static Fluorescence Quenching of Tryptophan. *Inorg. Chem.* **2018,** *57* (9), 4791-4794.
23. Trapaidze, A.; Hureau, C.; Bal, W.; Winterhalter, M.; Faller, P., Thermodynamic Study of Cu2+ Binding to the DAHK and GHK Peptides by Isothermal Titration Calorimetry (ITC) with the Weaker Competitor Glycine. *J. Biol. Inorg. Chem.* **2012,** *17* (1), 37-47.
24. Hureau, C.; Eury, H.; Guillot, R.; Bijani, C.; Sayen, S.; Solari, P.-L.; Guillon, E.; Faller, P.; Dorlet, P., X-ray and Solution Structures of CuIIGHK and CuIIDAHK Complexes: Influence on Their Redox Properties. *Chem. - Eur. J.* **2011,** *17* (36), 10151-10160.

25. Margerum, D. W., Dukes, G. R. , Kinetics and Mechanisms of Metal-ion and Proton-transfer Reactions of Oligopeptide Complexes. *Met. Ions Biol. Syst.* **1974,** *1*, 157-207.
26. Stefaniak, E.; Bal, W., CuII Binding Properties of N-Truncated Aβ Peptides: In Search of Biological Function. *Inorg. Chem.* **2019,** *58* (20), 13561-13577.
27. Snyder, S. W.; Ladror, U. S.; Wade, W. S.; Wang, G. T.; Barrett, L. W.; Matayoshi, E. D.; Huffaker, H. J.; Krafft, G. A.; Holzman, T. F., Amyloid-beta Aggregation: Selective Inhibition of Aggregation in Mixtures of Amyloid with Different Chain Lengths. *Biophys. J.* **1994,** *67* (3), 1216-1228.
28. Kim, D.; Kim, N. H.; Kim, S. H., 34 GHz Pulsed ENDOR Characterization of the Copper Coordination of an Amyloid β Peptide Relevant to Alzheimer's Disease. *Angewandte Chemie, International Edition in English* **2013,** *52* (4), 1139-1142.
29. Damante, C. A.; Osz, K.; Nagy, Z.; Pappalardo, G.; Grasso, G.; Impellizzeri, G.; Rizzarelli, E.; Sóvágó, I., The metal loading ability of beta-amyloid N-terminus: a combined potentiometric and spectroscopic study of copper(II) complexes with beta-amyloid(1-16), its short or mutated peptide fragments, and its polyethylene glycol (PEG)-ylated analogue. *Inorg. Chem.* **2008,** *47* (20), 9669-9683.
30. Drew, S. C.; Barnham, K. J., The Heterogeneous Nature of Cu(2+) Interactions with Alzheimer's Amyloid-β Peptide. *Acc. Chem. Res.* **2011,** *44* (11), 1146-1155.
31. Karr, J. W.; Szalai, V. A., Role of Aspartate-1 in Cu(II) binding to the Amyloid-b peptide Alzheimer's disease. *J. Am. Chem. Soc.* **2007,** *129*, 3796-3797.
32. Kowalik-Jankowska, T.; Ruta, M.; Wisniewska, K.; Lankiewicz, L., Coordination abilities of the 1-16 and 1-28 fragments of b-amyloid peptide towards copper(II) ions: a combined potentiometric and spectroscopic study. *J. Inorg. Biochem.* **2003,** *95*, 270-282.
33. Hong, L.; Carducci, T. M.; Bush, W. D.; Dudzik, C. G.; Millhauser, G. L.; Simon, J. D., Quantification of the binding properties of Cu2+ to the amyloid beta peptide: coordination spheres for human and rat peptides and implication on Cu2+-induced aggregation. *J. Phys. Chem. B.* **2010,** *114* (34), 11261-11271.
34. Shin, B.-K.; Saxena, S., Substantial Contribution of the Two Imidazole Rings of the His13 His14 Dyad to Cu(II) Binding in Amyloid-β(1 16) at Physiological pH and Its Significance. *Journal of Physical Chemistry A* **2011,** *115* (34), 9590-9602.
35. Kirsipuu, T.; Zadorožnaja, A.; Smirnova, J.; Friedemann, M.; Plitz, T.; Tõugu, V.; Palumaa, P., Copper(II)-binding equilibria in human blood. *Sci. Rep.* **2020,** *10* (1), 5686.
36. Bal, W.; Sokołowska, M.; Kurowska, E.; Faller, P., Binding of transition metal ions to albumin: sites, affinities and rates. *Biochimica et Biophysica Acta* **2013,** *1830* (12), 5444-5455.
37. Gonzalez, P.; Bossak, K.; Stefaniak, E.; Hureau, C.; Raibaut, L.; Bal, W.; Faller, P., N-terminal Cu Binding Motifs Xxx-Zzz-His (ATCUN) and Xxx-His and their derivatives: Chemistry, Biology and Medicinal Applications. *Chem. Eur. J.* **2018,** *24* (32), 8029-8041.
38. Perrone, L.; Mothes, E.; Vignes, M.; Mockel, A.; Figueroa, C.; Miquel, M. C.; Maddelein, M. L.; Faller, P., Copper transfer from Cu-Abeta to human serum albumin inhibits aggregation, radical production and reduces Abeta toxicity. *ChemBioChem* **2010,** *11* (1), 110-118.
39. Wezynfeld, N. E.; Stefaniak, E.; Stachucy, K.; Drozd, A.; Płonka, D.; Drew, S. C.; Krężel, A.; Bal, W., Resistance of Cu(Aβ4 - 16) to Copper Capture by Metallothionein-3 Supports a Function for the Aβ4 - 42 Peptide as a Synaptic Cu II Scavenger. *Angew. Chem. Int. Ed.* **2016,** *55* (29), 8235-8238.
40. Mital, M.; Wezynfeld, N. E.; Frączyk, T.; Wiloch, M. Z.; Wawrzyniak, U. E.; Bonna, A.; Tumpach, C.; Barnham, K. J.; Haigh, C. L.; Bal, W.; Drew, S. C., A Functional Role for Aβ in Metal Homeostasis? N-Truncation and High-Affinity Copper Binding. *Angew. Chem. Int. Ed.* **2015,** *54* (36), 10460-10464.
41. Viles, J. H.; Barritt, J. D.; Younan, N. D., N-Terminally Truncated Amyloid-β(11-40/42) Co-Fibrillises with its Full-Length Counterpart, Implications for Alzheimer's Disease. *Angew. Chem. Int. Ed.* **2017,** *56*, 9816-9819.
42. Barritt, J. D.; Viles, J. H., Truncated Amyloid-β(11-40/42) from Alzheimer Disease Binds Cu2+ with a Femtomolar Affinity and Influences Fiber Assembly. *Journal of Biological Chemistry* **2015,** *290* (46), 27791-27802.
43. Karr, J. W.; Akintoye, H.; Kaupp, L. J.; Szalai, V. A., N-Terminal deletions modify the Cu2+ binding site in amyloid-beta. *Biochemistry* **2005,** *44* (14), 5478-5487.
44. Borghesani, V.; Alies, B.; Hureau, C., Cu(II) binding to various forms of amyloid-β peptides. Are they friends or foes ? *European Journal of Inorganic Chemistry* **2018**, 7-15.
45. Teng, X.; Stefaniak, E.; Girvan, P.; Kotuniak, R.; Płonka, D.; Bal, W.; Ying, L., Hierarchical binding of copperII to N-truncated Aβ4–16 peptide. *Metallomics* **2020,** *12* (4), 470-473.
46. Esmieu, C.; Ferrand, G.; Borghesani, V.; Hureau, C., Impact of N-Truncated Aβ Peptides on Cu- and Cu(Aβ)-Generated ROS: CuI Matters! *Chemistry – A European Journal* **2021,** *27* (5), 1777-1786.
47. Pickart, L.; Margolina, A., Regenerative and Protective Actions of the GHK-Cu Peptide in the Light of the New Gene Data. *International journal of molecular sciences* **2018,** *19* (7), 1987.
48. Ma, W. H.; Li, M.; Ma, H. F.; Li, W.; Liu, L.; Yin, Y.; Zhou, X. M.; Hou, G., Protective effects of GHK-Cu in bleomycin-induced pulmonary fibrosis via anti-oxidative stress and anti-inflammation pathways. *Life sciences* **2020,** *241*, 117139.
49. Wang, X.; Liu, B.; Xu, Q.; Sun, H.; Shi, M.; Wang, D.; Guo, M.; Yu, J.; Zhao, C.; Feng, B., GHK-Cu-liposomes accelerate scald wound healing in mice by promoting cell proliferation and angiogenesis. *Wound Repair and Regeneration* **2017,** *25* (2), 270-278.
50. Bossak-Ahmad, K.; Wiśniewska, M. D.; Bal, W.; Drew, S. C.; Frączyk, T., Ternary Cu(II) Complex with GHK Peptide and Cis-Urocanic Acid as a Potential Physiologically Functional Copper Chelate. *Int J Mol Sci* **2020,** *21* (17), 6190.
51. Wezynfeld, N. E.; Tobolska, A.; Mital, M.; Wawrzyniak, U. E.; Wiloch, M. Z.; Płonka, D.; Bossak-Ahmad, K.; Wróblewski, W.; Bal, W., Aβ5–x Peptides: N-Terminal Truncation Yields Tunable Cu(II) Complexes. *Inorg. Chem.* **2020,** *59* (19), 14000-14011.
52. Stoll, S.; Schweiger, A., *Journal of Magnetic Resonance* **2006,** *178*, 42-55.
53. Sokołowska, M.; Bal, W., Cu(II) complexation by "non-coordinating" N-2-hydroxyethylpiperazine-N′-2-ethanesulfonic acid (HEPES buffer). *Journal of Inorganic Biochemistry* **2005,** *99* (8), 1653-1660.
54. Dorlet, P.; Gambarelli, S.; Faller, P.; Hureau, C., Pulse EPR Spectroscopy Reveals the Coordination Sphere of Copper(II) Ions in the 1–16 Amyloid-b Peptide:AKey Role of the First Two N-Terminus Residues. *Angewandte Chemie, International Edition in English* **2009,** *48* (49), 9273-9276.
55. Drew, S. C.; Noble, C. J.; Masters, C. L.; Hanson, G. R.; Barnham, K. J., Pleomorphic copper coordination by Alzheimer's disease amyloid-beta peptide. *Journal of the American Chemical Society* **2009,** *131* (3), 1195-1207.
56. Crans, D. C.; Ehde, P. M.; Shin, P. K.; Pettersson, L., Structural and kinetic characterization of simple complexes as models for vanadate-protein interactions. *Journal of the American Chemical Society* **1991,** *113* (10), 3728-3736.
57. Crans, D. C.; Kostenkova, K., Open questions on the biological roles of first-row transition metals. *Communications Chemistry* **2020,** *3* (1), 104.
58. Peisach, J.; Blumberg, W. E., Structural implications derived from the analysis of electron paramagnetic resonance spectra of natural and artificial copper proteins. *Archives of Biochemistry and Biophysics* **1974,** *165* (2), 691-708.
59. Jiang, F.; McCracken, J.; Peisach, J., Nuclear quadrupole interactions in copper(II)-diethylenetriamine-substituted

imidazole complexes and in copper(II) proteins. *Journal of the American Chemical Society* **1990,** *112* (25), 9035-9044.
60. Branch, T.; Girvan, P.; Barahona, M.; Ying, L., Introduction of a Fluorescent Probe to Amyloid-β to Reveal Kinetic Insights into Its Interactions with Copper(II). *Angewandte Chemie International Edition* **2015,** *54* (4), 1227-1230.
61. Pedersen, J. T.; Teilum, K.; Heegaard, N. H. H.; Østergaard, J.; Adolph, H.-W.; Hemmingsen, L., Rapid Formation of a Preoligomeric Peptide–Metal–Peptide Complex Following Copper(II) Binding to Amyloid β Peptides†. *Angewandte Chemie, International Edition in English* **2011,** *50* (11), 2532-2535.
62. Sóvágó, I.; Kállay, C.; Várnagy, K., Peptides as complexing agents: Factors influencing the structure and thermodynamic stability of peptide complexes. *Coordination Chemistry Reviews* **2012,** *256* (19), 2225-2233.
63. Kotuniak, R.; Strampraad, M. J. F.; Bossak-Ahmad, K.; Wawrzyniak, U. E.; Ufnalska, I.; Hagedoorn, P.-L.; Bal, W., Key Intermediate Species Reveal the Copper(II)-Exchange Pathway in Biorelevant ATCUN/NTS Complexes. *Angewandte Chemie International Edition* **2020,** *59* (28), 11234-11239.
64. Guilloreau, L.; Damian, L.; Coppel, Y.; Mazarguil, H.; Winterhalter, M.; Faller, P., Structural and thermodynamical properties of CuII amyloid-beta16/28 complexes associated with Alzheimer's disease. *Journal of Biological Inorganic Chemistry* **2006,** *11* (8), 1024-1038.
65. Rózga, M.; Sokołowska, M.; Protas, A. M.; Bal, W., Human Serum Albumin Coordinates Cu(II) at its N-terminal Binding Site with 1 pM Affinity. *J. Biol. Inorg. Chem.* **2007,** *12* (6), 913-918.
66. Sokolowska, M.; Krezel, A.; Dyba, M.; Szewczuk, Z.; Bal, W., Short peptides are not reliable models of thermodynamic and kinetic properties of the N-terminal metal binding site in serum albumin. *European Journal of Biochemistry* **2002,** *269* (4), 1323-1331.

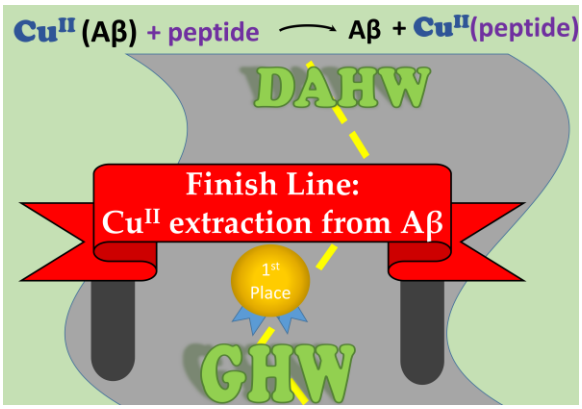

TOC synopsis: We discuss and report the interpeptidic Cu^{II} exchange rate constants between $Cu(A\beta_{1-16})$ and $Cu(A\beta_{1-28})$ to fluorescent peptides GHW and DAHW by use of a quantitative tryptophan fluorescence quenching method. These rate constants range from 0.81 to 4.4 x 10^4 $M^{-1}s^{-1}$ and vary depending on variables such as the length of the Aβ peptide, the Cu(Aβ) coordination chemistry, the location of His residues in GHW and DAHW, and the pH.